The nature of the near-infrared core source in 3C 433

Edgar A. Ramírez,[1]⋆ C. N. Tadhunter,[1] D. Axon,[2] D. Batcheldor,[2] S. Young,[2]
C. Packham[3] and W. B. Sparks[4]

[1]*Department of Physics and Astronomy, University of Sheffield, Sheffield S3 7RH*
[2]*Department of Physics, Rochester Institute of Technology, 85 Lomb Memorial Drive, Rochester, NY 14623, USA*
[3]*Department of Astronomy, University of Florida, 211 Bryant Science Center, PO Box 112055, Gainesville, FL 32611-2055, USA*
[4]*Space Telescope Science Institute, 3700 San Martin Drive, Baltimore, MD 21218, USA*

ABSTRACT

We report the analysis of near-infrared (near-IR) imaging, polarimetric and spectroscopic observations of the powerful radio galaxy 3C 433 ($z = 0.1016$), obtained with the *Hubble Space Telescope* (*HST*) and the United Kingdom Infrared Telescope. The high spatial resolution of *HST* allows us to study the near-nuclear regions of the galaxy (<1 kpc). In line with previous observations, we find that 3C 433 has an unresolved core source that is detected in all near-IR bands, but dominates over the host galaxy emission at 2.05 μm.

Our analysis reveals (1) the presence of a dust lane aligned close to the perpendicular [position angle (PA) = $70° \pm 5°$] to the inner radio jet axis (PA = $-12° \pm 2°$), (2) a steep slope to the near-IR spectral energy distribution (SED; $\alpha = 5.8 \pm 0.1$; $F_\nu \propto \nu^{-\alpha}$), (3) an apparent lack of broad permitted emission lines at near-IR wavelengths, in particular the absence of a broad Paα emission line and (4) high intrinsic polarization for the unresolved core nuclear source (8.6 ± 1 per cent), with an E-vector perpendicular (PA = $83°.0 \pm 2°.3$) to the inner radio jet. Using five independent techniques, we determine an extinction to the compact core source in the range $3 < A_V < 67$ mag.

An analysis of the long wavelength SED rules out a synchrotron origin for the high near-IR polarization of the compact core source. Therefore, scattering and dichroic extinction are plausible polarizing mechanisms, although in both of these cases the broad permitted lines from the active galactic nuclei are required to have a width $>10^4$ km s^{-1} (full width at half-maximum) to escape detection in our near-IR spectrum. Dichroic extinction is the most likely polarization mechanism because it is consistent with the various available extinction estimates. In this case, a highly ordered, coherent toroidal magnetic field must be present in the obscuring structure close to the nucleus.

Key words: techniques: polarimetric – galaxies: active – galaxies: individual: 3C 433 – infrared: galaxies.

1 INTRODUCTION

In the unified schemes for radio-loud active galactic nuclei (AGN), radio galaxies and quasars are deemed to be the same objects viewed from different lines of sight (Barthel 1989). Some of the best evidence to support such orientation-based unified schemes is provided by spectropolarimetry observations of radio galaxies that show broad permitted lines in the polarized spectrum, characteristic of scatter quasar light (Ogle et al. 1997; Cohen et al. 1999).

A key element of the standard unified schemes is a central obscuring torus, with an axis parallel to the radio axis. This torus obscures structures close to the nucleus, such as the broad-line region [BLR: $r < 1$ pc, full width at half-maximum (FWHM) $\approx 10^3 - 10^4$ km s^{-1}] and the main optical/ultraviolet continuum generating region in the accretion disc. However, despite its status as a fundamental element of the unified scheme, large uncertainties remain about the structure of the torus and the degree of extinction it induces.

Apart from helping to clarify the apparent differences among radio-loud AGN, the circumnuclear dust and its spatial distribution are directly affected by phenomena occurring close to the nucleus, such as circumnuclear outflows. Hence, the study of the distribution and properties of the dust is important for understanding the impact of the nuclear activity on the host galaxies.

Because AGN are embedded in dusty regions and surrounded by a dust torus, observations at near-infrared (near-IR) wavelengths

⋆E-mail: e.ramirez@sheffield.ac.uk

are crucial, due to the relatively low extinction suffered at such wavelengths. The advantages of observing radio galaxies at near-IR wavelengths have been demonstrated by imaging observations of Cygnus A (Djorgovski et al. 1991; Tadhunter et al. 1999) and PKS 0634−205 (Simpson, Ward & Wilson 1995), which show a progression from resolved galaxy-like structures at short near-IR wavelengths to unresolved point sources at longer wavelengths. These results have been interpreted in terms of the quasars shining through the obscuring dust torus. In this case, it should be possible to directly detect the BLR associated with the AGN at near-IR wavelengths. Indeed, previous near-IR spectroscopic observations have shown that some radio galaxies originally classified as narrow-line radio galaxies (NLRG) present a broad Paα line in the K band (Hill, Goodrich & DePoy 1996; Holt et al. 2006). This provides evidence for a hidden broad-emission-line region and gives support to the orientation-based unified schemes.

3C 433 ($z = 0.1016$; Schmidt 1965) is a powerful radio galaxy that has been classified as an NLRG at optical wavelengths (Koski 1978), and shows signs of a young stellar population in its optical continuum emission (Wills et al. 2002; Holt et al. 2007). With a radio structure comprising jet and knot structures close to the nucleus, as well as hotspots and distorted radio lobes on larger scales (van Breugel et al. 1983), its Fanaroff and Riley (FR) classification is uncertain, but it is more commonly identified as an Fanaroff–Riley type II (FR II) source. The existing optical *Hubble Space Telescope* (*HST*) images taken with the F702W filter show a complex central structure attributed to dust obscuration and possible star-forming regions (de Koff et al. 1996), but no sign of an unresolved optical nucleus (Chiaberge, Capetti & Celotti 1999). In contrast, 3C 433 has an unusually bright compact nuclear source at near-IR wavelengths (Madrid et al. 2006), as well as exceptionally red near-IR colours (Lilly, Longair & Miller 1985). At mid-IR wavelengths, Spitzer observations of 3C 433 indicate the existence of a hidden quasar obscured by dust (Ogle, Whysong & Antonucci 2006). Therefore, this object provides an excellent opportunity to investigate the nature of compact near-IR core sources in AGN.

In this article, we analyse photometric and polarimetric imaging observations of the nuclear region of 3C 433 obtained with the Near-Infrared Camera and Multi Object Spectrograph (NICMOS) on the *HST*. We also present near-IR spectra taken with the United Kingdom Imaging Spectrometer (UIST) Integral Field Unit (IFU) on the United Kingdom Infrared Telescope (UKIRT). These data allow us to examine the nature of the nuclear point source using a range of techniques: photometry, spectroscopy and polarimetry. We analyse the results of these techniques together, and discuss them in the context of the orientation-based unified schemes.

In Section 2, we describe the observations, as well as the data reduction procedures. We present the analysis in Section 3 and in Section 4 we discuss the results in terms of the nature of the circumnuclear structures. In Section 5, we present the conclusions.

Throughout this paper, we assume the following cosmological parameters: $H_0 = 73 \, \mathrm{km \, s^{-1} \, Mpc^{-1}}$, $\Omega_M = 0.3$ and $\Omega_\Lambda = 0.7$.

2 OBSERVATIONS AND DATA REDUCTION

2.1 *HST* images

The *HST* images were obtained during Cycle 13 on 2005 August 19 (GO 10410, PI: C. N. Tadhunter), using the NICMOS1 camera (NIC1) with the F110W, F145M, F170M filters (central wavelengths: 1.025, 1.45 and 1.7 µm, respectively), and with the NICMOS2 (NIC2) camera using the Long Polarizer (POL-L) fil-

ters centred at 2.05 µm. In the latter case, three polarization filter images (POL0L, POL120L and POL240L), whose principal axes of transmission are separated by 120°, were obtained to derive polarimetric information; these were also co-added to form a deep 2.05 µm image.

The observations were coordinated in a parallel way: observations of 3C 433 in NIC1 were made when NIC2 chopped to the sky. The standard X-STRIP-DITHER-CHOP pattern (Barker et al. 2007) was used for the observations in order to facilitate accurate subtraction of the sky emission, with a total of eight positions (four sky, four objects), a chop throw of 31.5 arcsec (in the Y-direction) and a spacing between the dithering positions of 0.9 arcsec (in the X-direction). The total on-source integration times were 768 s at 1.025, 1.45 and 1.7 µm, and 624 s at 2.05 µm.

The *HST* data were reduced using the standard NICMOS calibration software CALNICA (MacLaughlin & Wiklind 2007). To obtain the polarization degree and PA using the NIC2 POL-L observations, the Stokes parameters of the polarimetric data were calculated and analysed according to the prescription of Sparks & Axon (1999), as follows. First, the mean and standard deviation of the intensity of each polarizer image were obtained through concentric apertures, centred in the galaxy's nucleus, using the IRAF task PHOT. Then, using an IDL routine, we obtained the Stokes parameters (I, U, Q), by solving the matrix of the linear system for three polarizers. The transmission coefficients for the POL-L polarizers were derived from data taken with the post-NICMOS Cooling System (Batcheldor et al. 2006). Finally, we derived our estimates of the polarized flux percentage (100 per cent $\times \sqrt{Q^2 + U^2}/I$) and the PA [$\frac{1}{2}\tan^{-1}(U/Q)$].

2.2 UKIRT spectra

In order to search for broad hydrogen emission lines associated with the hidden AGN, we have also analysed spectroscopic data taken with the UIST IFU imaging spectrometer on UKIRT.

The observations were obtained with the HK grism on 2003 September 16. The air mass ranged from 1.089 at the beginning of the observations to 1.661 at the end. The bandpass extended from 1.41 to 2.53 µm, and a mean velocity resolution of $\approx 160 \, \mathrm{km \, s^{-1}}$ was achieved. The data were taken in the standard ABBA pattern, with the telescope nodding between the galaxy and sky positions.

The UKIRT data were reduced in the standard way using IRAF. First, we combined the galaxy and sky frames separately, using a median filter to remove cosmic rays; then we subtracted sky from galaxy frames to correct for the sky emission, bias and dark current. Residual hot pixels were removed using the FIXPIX task, and the spectra were wavelength calibrated using argon arc frames. The flux calibration was achieved by dividing by a wavelength calibrated spectrum of the type A0V atmospheric standard star HD34317, observed close in time to the 3C 433 observations; the air mass ranged from 1.47 to 1.45. Finally, the data were multiplied by the spectrum of a blackbody of temperature 9480 K to produce a flux- and wavelength-calibrated spectrum. The spectroscopic analysis presented below focuses on the combined spectrum for a 2 × 1 arcsec aperture centred on the nucleus.

3 ANALYSIS

3.1 *HST* imaging

At radio wavelengths 3C 433 is dominated by the extended radio jet and lobes, whereas at optical wavelengths it is dominated by
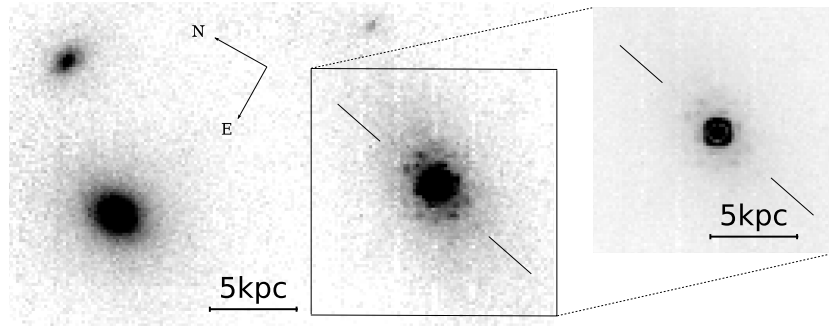
Figure 1. Near-IR images of 3C 433 at 2.05 μm. The image on the left shows a 13.30 × 7.7 arcsec field with 3C 433 inside the square; the north and north-east companion galaxies lie to the left-hand side, whereas in the upper-right side lies a patch of emission. The image on the right displays 3C 433 with a different contrast to show the point source quality of the nuclear region. The radio jet orientation is indicated by the pair of lines.

the stellar light of the host galaxy, albeit with a disturbed morphology (de Koff et al. 1996) and signs of recent star formation (Holt et al. 2007). In this work, on the other hand, we find that at near-IR wavelengths 3C 433 has a bright unresolved point-like nucleus that clearly dominates over the host galaxy emission (see Fig. 1). At 2.05 μm, the nuclear source shows distinctly the prominent first Airy ring and also some signs of the second Airy ring. This detection of an unresolved source makes it clear that, using near-IR observations, we are able to penetrate the circumnuclear dust material. In addition, our 2.05 μm POL-L images also detect the nearby companion galaxies 7.8 arcsec to the north-east, and 9.5 arcsec to the north of 3C 433 (see also van Breugel et al. 1983), as well the fainter patch of emission 4.1 arcsec to the north-west of 3C 433, detected before by de Koff et al. (1996).

To estimate the flux of the galaxy core at each wavelength, a trial and error subtraction of point spread functions (PSFs) generated by the TINY TIM software (Krist & Hook 2004) was performed. The artificial PSFs were recentred and scaled by different factors to obtain the best subtraction. We consider that the best factor is obtained when, after PSF subtraction, the residual PSF structure is minimized. The fluxes of the scaled PSFs were measured using the GAIA program in the STARLINK software library. The core fluxes derived from this procedure are listed in Table 1.

While the 2.05 μm image is dominated by an unresolved point source, at shorter wavelengths (1.025 μm), using the resolution of *HST* (0.1 arcsec) it is possible to detect for the first time a kpc-scale dust lane. In Fig. 2, we compare the 1.025 μm image before and after PSF subtraction. The PA of the dust lane is PA = 70° ± 5°. For comparison, the inner jet axis defined by the compact core components C1 and C2, detected in the 8.465 GHz map of Black et al. (1992), has PA = −12° ± 2°, whereas the outer jet axis, defined by components S1 and N1 from Black et al. (1992), has PA = −14°.0 ± 0°.5. Therefore, the PA of the dust lane is offset by 82° ± 5° relative to the inner jet, and 84° ± 5° with respect to the outer jet.

Table 1. Core fluxes for 3C 433 measured from *HST*/NICMOS images.

Filter	Central wavelength of the bandpass (μm)	Flux density (Jy)
F110W	1.025	$(2.8 \pm 0.7) \times 10^{-5}$
F145M	1.45	$(1.5 \pm 0.1) \times 10^{-4}$
F170M	1.7	$(4.8 \pm 0.3) \times 10^{-4}$
POL-L	2.05	$(1.6 \pm 0.2) \times 10^{-3}$

3.1.1 Polarimetry

Using an aperture of 0.9 arcsec diameter centred on the nuclear source (this contains the first Airy ring), we derive a relatively high linear polarization of $P_{2.05} = 7.0 \pm 0.2$ per cent. The same analysis applied to the nucleus of the brighter north-east companion galaxy gives $P_{2.05} = 0.5 \pm 1$ per cent. This demonstrates that the high near-IR polarization measured in the nucleus of 3C 433 is not due to systematic or calibration errors. Note that, due to the dominance of the PSF of the nuclear point source, we have not been able to measure significant spatially resolved polarization in the halo of the galaxy.

The degree of polarization is underestimated because unpolarized starlight from the host galaxy dilutes the intrinsic AGN polarization. We have estimated the host galaxy starlight contribution in the following two ways. First, we measured the starlight contribution from the 1.025 μm image[1] following subtraction of the best-fitting PSF for the point source, then extrapolated to 2.05 μm using the typical colours for radio galaxies hosts from Lilly et al. (1985). This yields a starlight contribution of 14 per cent to the total flux at 2.05 μm. Secondly, we have measured the starlight contribution directly from the PSF-subtracted 2.05 μm image, giving a starlight contribution of 23 per cent. Both methods used a 0.9 arcsec diameter aperture. Assuming that the starlight is itself unpolarized and contributes 14–23 per cent of the total light in the polarimetric aperture, we therefore estimate an intrinsic polarization of $P_{2.05}^{\rm int} = 8.6 \pm 1$ per cent for the point source.

The PA of the E-vector for the nuclear point source is $83° \pm 2°.3$, offset by $95° \pm 3°$ relative to the inner radio jet and $97° \pm 2°.3$ relative to the outer radio jet. That is, the radio axis and 2.05 μm band polarization vector are close to perpendicular within the estimated uncertainty.

3.1.2 SED and extinction

The spectral energy distribution (SED) of 3C 433 is shown in Fig. 3. Clearly, the flux from the nuclear point source shows a steep decline towards shorter wavelengths in the near-IR. Fitting a power law to the *HST*/NICMOS core fluxes ($F_\nu \propto \nu^{-\alpha}$, $F_\lambda \propto \lambda^{\alpha-2}$), we obtain a spectral index $\alpha = 5.8 \pm 0.1$.

---

[1] Since the AGN point source contributes least at the shorter wavelengths, the 1.025 μm image can potentially provide the most accurate measure of the starlight contribution, although additional uncertainties arise because of the need to extrapolate from 1.025 to 2.05 μm.
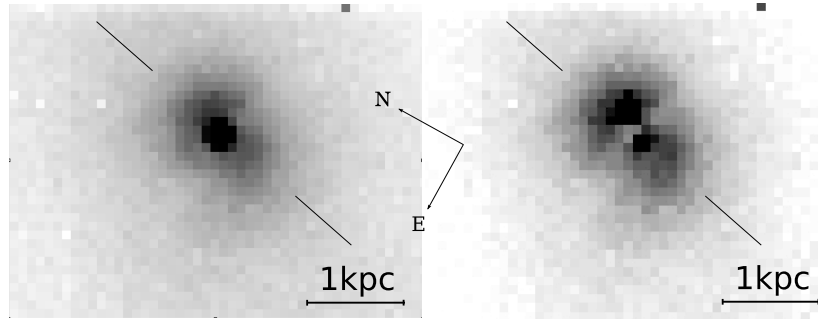
Figure 2. Images of the central region of 3C 433 at 1.025 μm. Left-hand panel: before PSF subtraction. Right-hand panel: after PSF subtraction. The pair of lines represents orientation of radio jets. A dust lane can be seen in both images, but is clearer in the right-hand image.
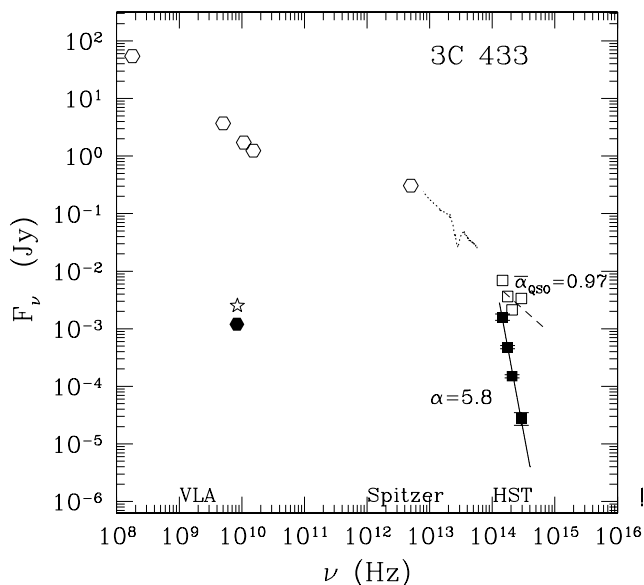
Figure 3. The SED of 3C 433. The *HST*/NICMOS fluxes of the unresolved core source are represented by filled squares; the solid straight line is the best power-law fit ($\alpha = 5.8 \pm 0.1$). The dashed line is the mean dereddened power law for quasars ($\overline{\alpha}_{QSO} = 0.97$: Simpson & Rawlings 2000). The open squares are the reddening corrected *HST*/NICMOS points. The open hexagons are radio Very Large Telescope (VLA) data from NED and the 60 μm far-IR flux from Impey & Gregorini (1993), respectively. The filled hexagon and the star are the radio emission from the southern radio core component of Hardcastle et al. (1998) and our own measurements, respectively. We have measured the VLA 8.465 GHz flux from the data published in (Black et al. 1992) of the south component of the radio core (C2), which is marginally more compact than the northern core component (Black et al. 1992), and coincident with the *Chandra* position of the nucleus (Miller & Brandt 2009). We find a 8.45 GHz flux of 2.53×10^{-3} Jy for the southern knot, the slightly discrepancy between our radio measurements and that of Hardcastle et al. (1998) is likely to be due to the fact that the Hardcastle et al. (1998) core flux has been corrected for contamination by the underlying radio jet. Finally, the doted line represents *Spitzer* Infrared Spectrograph data (Ogle et al. 2006).

In order to derive the degree of reddening of the nuclear point source, we have used five different techniques.

(1) Near-IR SED. The dereddening necessary to make the measured near-IR slope consistent with a quasar spectrum ($-0.67 < \alpha < 1.62$, with $\overline{\alpha}_{QSO} = 0.97$; Simpson & Rawlings 2000) was estimated. This method gives an extinction $A_{2.05\,\mu m} = 1.6 \pm^{0.6}_{0.2}$ mag. Extrapolating to optical wavelengths using a typical Galactic ex-

tinction law ($A_{2.05\,\mu m}/A_V = 0.107$; Mathis 1990) and correcting for Galactic extinction ($A_V = 0.68$ mag; Schlegel, Finkbeiner & Davis 1998), $A_V = 14 \pm^6_2$ mag is obtained.

(2) X-ray luminosity. We estimated the 1.0 μm luminosity using the X-ray to near-IR correlation in Kriss (1988) and the nuclear luminosity of 3C 433 at 2keV determined by Hardcastle, Evans & Croston (2009, see also Miller & Brandt 2009) from *Chandra* data. Next, we find $F_{1.025\,\mu m}$, taking the luminosity distance of 444 Mpc [from NSA/IPAC extragalactic database (NED)]. By comparing this flux to our observed 1.025 μm flux, we derive an extinction of $A_{1.025\,\mu m} = 6.2 \pm 0.4$ mag. Finally, $A_V = 17.8 \pm 1.1$ mag is obtained using the extinction law of Mathis (1990).

(3) X-ray column. The atomic hydrogen column density derived from *Chandra* data is $N_H = 9 \pm 1 \times 10^{22}$ cm^{-2} (Hardcastle et al. 2009). Using the standard Galactic ratio $A_V/N_H = 5.3 \times 10^{-22}$ mag cm^2 (Bohlin, Savage & Drake 1978), $A_V = 48 \pm 5$ mag is obtained. However, given that AGN generally have dust to gas ratios that are significantly lower than Galactic (Maiolino et al. 2001), this is likely to represent an upper limit. We have used the results from Maiolino et al. (2001) shown in his fig. 1, to calculate the upper and lower limits of true dust extinction. Referring to fig. 1. of Maiolino et al. (2001), we calculated the mean E_{B-V}/N_H ratio of the seven upper AGN below the Galactic standard and the mean of the ratio of the lower points, both using the Astrophysics Data System's data extractor DEXTER (Demleitner et al. 2001). With these two mean ratios, we find that the true dust extinction is likely to fall in the range $3 < A_V < 17$ mag.

(4) Near-IR polarization. Under the assumption that the measured intrinsic near-IR polarization is due to dichroic extinction by near-nuclear dust structures, the correlation between the observed linear polarization in the *K* band and the optical extinction (Jones 1989) yields $15 < A_V < 67$ mag, i.e. consistent with our previous estimates of A_V.

(5) Silicate absorption. The *Spitzer* IR spectrum shows a deep silicate absorption line at 9.7 μm, with an optical depth of $\tau_{9.7} = 0.71 \pm 0.07$ (Ogle et al. 2006). Using the empirically derived relationship between optical extinction and silicate absorption strength ($A_V/\tau_{9.7} = 18.5 \pm 1$; Whittet 1987), we find $A_V = 13.1 \pm 3.3$.

The various extinction estimates are compared in Table 2. Overall, given the uncertainties inherent in all the techniques, there is a remarkable degree of agreement. The similarity between the extinction estimated using the dichroic method and the other extinction estimates supports a dichroic origin of the polarization (see the Discussion). However, scattering processes can also make an important contribution to the polarization.

Table 2. Extinction estimates for the core source in 3C 433, based on various methods . The results are compared with those obtained for Cygnus A using the same methods.

No. method	Method	A_V (mag) 3C 433	Cygnus A
1	Near-IR SED	$14 \pm^{6}_{2}$	–
2	X-ray luminosity	18 ± 1	107
3	X-ray column	3–17	11–69
4	Near-IR polarization	15–67	50–324
5	Silicate absorption	13 ± 3	–

3.2 UKIRT spectroscopy

Despite the strength of the near-IR continuum from the unresolved AGN, the UKIRT spectrum of the nucleus shows no clear evidence for a strong broad Paα line. After removing telluric absorption features, a narrow Paα ($\lambda_0 = 1.8756\,\mu$m) emission line is present at the expected redshifted wavelength ($\approx 2.07\,\mu$m; see Fig. 4).

This lack of a broad line is unexpected, and stands out for the following reasons. Our near-IR results suggest that we are able to look through the dust torus directly into the AGN. A strong broad Paα line should thus be present. Moreover, a prominent broad Paα is detected in the spectra of other powerful radio galaxies with obscured quasar nuclei (e.g. PKS 1549−79; Holt et al. 2006).

Although we do not detect a broad Paα line directly in our spectra, we can estimate the ranges of Paα equivalent width (EW) and FWHM that are consistent with the non-detection. This was done by adding broad Gaussian lines of various velocity widths (FWHM = 5000, 10 000 and 15 000 km s^{-1}) and EWs (50, 100 and 150 Å) to our spectrum at the expected wavelength of Paα, and then examining whether the line could be clearly detected above the continuum upon visual inspection of the plots (see Fig. 5). Note that the EWs of the broad Paα line in optically obscured and unobscured quasar nuclei generally fall in the range $50 < \text{EW}_{\text{Pa}\alpha} < 170$ Å (Rudy & Tokunaga 1982; Holt et al. 2006; Landt et al. 2008).
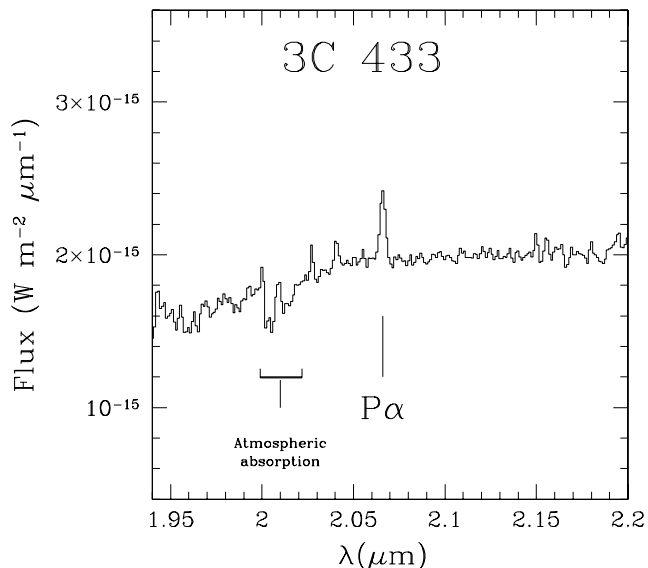
Figure 4. Near-IR UKIRT/UIST spectrum of the radio galaxy 3C 433 from 1.94 to 2.2 μm. The position of the narrow Paα line is marked. Residual atmospheric absorption features are visible around 2.0 μm that were not completely removed by division by the telluric standard star spectrum. Note the lack of any clear evidence for a broad Paα feature.

On the basis of Fig. 5, the non-detection of broad Paα is favoured by a large FWHM and a small EW. If the AGN in 3C 433 has a broad Paα line with EW typical of the AGN (median EW ≈ 92 Å: Landt et al. 2008), its Paα must have a velocity width $> 10\,000$ km s^{-1} to escape detection. Such large velocity widths, while not typical of AGN in general, are commonly measured in broad-line radio-loud AGN in the local Universe, which have radio and emission line luminosities similar to 3C 433 (e.g. the BLRG in Osterbrock, Koski & Phillips 1976; Buttiglione et al. 2009). Therefore, the simplest explanation for the non-detected broad Paα in 3C 433 is that it contains a typical BLRG nucleus with FWHM $> 10\,000$ km s^{-1}.

4 DISCUSSION

We have found that 3C 433 shows several interesting characteristics at near-IR wavelengths. In this section, we summarize and discuss our results.

(i) An unresolved point-like nucleus is detected at all near-IR wavelengths. This source dominates over the starlight from the host galaxy in the 2.05 μm band. The strength of the nuclear point source suggests that we are looking directly at the AGN through the circumnuclear dust.

(ii) It is plausible that the kpc-scale dust lane that falls close to perpendicular to the inner radio jet ($\Delta\theta = 82° \pm 5°$) forms the outer part of a torus structure responsible for the nuclear obscuration.[2]

(iii) The extinction obtained using the different methods is consistent with a relatively modest obscuration of the nuclear point source ($3 < A_V < 67$ mag), compared with the archetypical powerful radio galaxy Cygnus A (Tadhunter et al. 1999).

(iv) We have found that the spectrum of 3C 433 lacks a strong broad Paα emission line. This is unexpected, because the IR images suggest that we are looking directly at the AGN. However, it is plausible that the non-detection is due to the fact that 3C 433 has a Paα line with a relatively large width (FWHM $> 10\,000$ km s^{-1}; typical of BLRG), which makes it difficult to detect in our spectra.

(v) The nucleus is highly polarized ($P^{\text{int}}_{2.05\,\mu\text{m}} = 8.6 \pm 1$ per cent) and the orientation of the polarization E-vector at near-IR wavelengths is close to perpendicular to the inner radio jet axis ($\Delta\theta = 95° \pm 3°$).

The polarization of the near-IR light could be produced by three mechanisms: (1) non-thermal synchrotron radiation; (2) scattering of the light due to dust or electrons or (3) dichroic extinction.

At first sight, it might be thought that the lack of a broad Paα line and the relatively high degree of polarization can be explained in terms of strong non-thermal synchrotron continuum emission swamping the emission lines at near-IR wavelengths. Indeed, Capetti et al. (2007) have proposed a synchrotron origin for the optical polarization measured in the unresolved optical cores of a sample of nine nearby FR I radio galaxies. Such interpretation is supported by the close correlations between the X-ray, optical and radio properties of the FR I cores (e.g. Balmaverde, Capetti & Grandi 2006). However, in 3C 433 a major contribution to the near-IR continuum emission from a synchrotron mechanism is unlikely for the following reasons. The SEDs produced by synchrotron

---

[2] Hereafter we refer to the 'circumnuclear obscuring region' as the 'dust torus'. Because there may exist dust on a continuous range of scales between the inner torus and outer kpc-dust lane, the division between torus and dust lane is largely semantic.
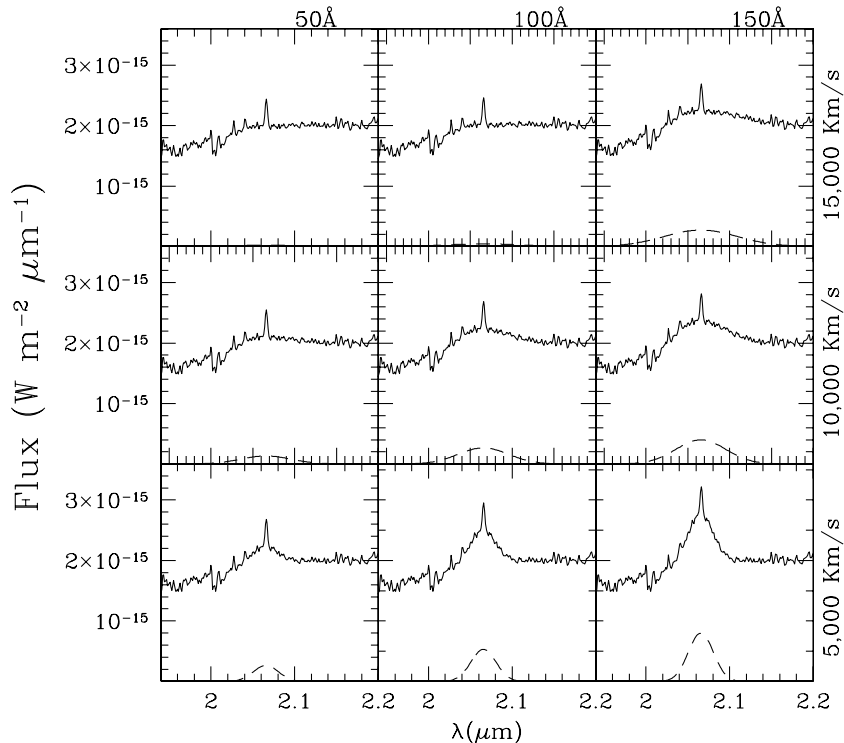
Figure 5. The SED of 3C 433 (solid lines) with added Gaussian profiles (dashed lines) representing broad Paα features with different EWs (columns) and FWHM (rows). For a typical quasar Paα EW (EW = 100 Å), it is difficult to detect the broad Paα line with these data if the lines has FWHM $\geq 10\,000\,\mathrm{km\,s^{-1}}$.

radiation from flat spectrum core radio sources generally show significant declines – by orders of magnitude – between the radio and the near-IR wavelengths (e.g. Dicken et al. 2008). A clear example is the quasar 3C 273, for which the flat spectrum radio core is two orders of magnitude brighter than its near-IR core flux. Moreover, the flat spectrum radio cores in lower luminosity FR I radio galaxies also have relatively steep spectra between radio and optical wavelengths ($\alpha \approx 0.6$–1.0; Balmaverde et al. 2006).[3] In contrast, a power-law fit between the radio core flux and the near-IR data for 3C 433 yields a flat or gently rising spectrum (see Fig. 3), with no decline between the radio and the near-IR wavelengths. Given that this is difficult to reconcile with the steep radio-IR SEDs of known synchrotron dominated core sources, it is unlikely that synchrotron radiation substantially dilutes the broad Paα feature.

Regarding scattering, we expect the scattered light to be polarized perpendicular to the radius vector from the illuminating source. We have found that the PA of the E-vector is close to parallel to the dust lane (offset = 13°0 ± 5°5) and perpendicular to the inner radio axis (offset = 95° ± 3°). Therefore, we could be seeing the light scattered by the inner face of the torus on the far side of the nucleus, or polar scattering by material above the torus. Potentially, scattered light could provide an alternative to explain the non-detection of broad Paα line, since if the scattering is by electrons and they are sufficiently hot ($>10^6\,\mathrm{K}$) then a very broad Paα line (FWHM $> 10\,000\,\mathrm{km\,s^{-1}}$) would not be detected in our spectroscopic data if it has an EW typical of quasars.

[3] Note that, in the case of the FR I sources, there is no evidence that the compact cores suffer substantial dust extinction at optical wavelengths (typical A_V between 0.15 and 3 mag: Chiaberge et al. 2002), and the X-ray absorption column densities in these sources are also relatively low (Balmaverde et al. 2006).

Dichroic extinction is the selective attenuation of light passing through a medium with dust grains that are aligned by a magnetic field. It has been found that the efficiency of this mechanism is low: large quantities of dust are required to produce a reasonable degree of polarized light (Jones 1989). In the case of 3C 433, the similarity between the extinction required to give the measured polarization at 2.05 μm and the other extinction estimates (see Table 2) provides strong evidence for a dichroic origin of the polarization. If this is the case, since the E-vector of the polarized light is aligned perpendicular to the radio axis, the dust grains in the torus must be aligned perpendicular to the torus plane and, therefore, the magnetic field must be parallel to the dust torus (i.e. the magnetic field is toroidal). This scheme requires the presence of elongated dust grains and the existence of a highly coherent magnetic fields in the torus. Indeed, for the dichroic mechanism to work the polarization efficiency is required to be close to the upper limit of that measured for stars in our galaxy (Jones 1989). This can be explained in terms of the fact that the circumnuclear torus is likely to be more compact and coherent structure than the large-scale disc of the Milky Way.

It is also interesting to compare our results for 3C 433 with those obtained for Cygnus A, the only other powerful radio source to have its near-IR core source investigated in such detail. We have recalculated the optical extinction in Cygnus A using the various methods applied in 3C 433, and tabulated the results in Table 2. By method (2), we obtain $A_V = 107$ mag, given the nuclear X-ray luminosity in Ueno et al. (1994). This optical extinction is slightly higher than the reported in Tadhunter et al. (1999; 93 mag), because the X-ray luminosity given by Ueno et al. (1994) is higher than the one taken in Tadhunter et al. (1999). By method (3), we estimate $A_V = 198$ mag, given the column density of $N_H = 3.75 \times 10^{23}\,\mathrm{cm^{-2}}$ (Ueno et al. 1994), and by applying the arguments of Maiolino et al. (2001) we get $A_V = 11$–69 mag. The intrinsic near-IR polarization measured in the unresolved core of Cygnus A is

$P_K = 28$ per cent, with an offset of $96°$ between the radio jet and the E-vector (Tadhunter et al. 2000). Under the assumptions of method (4), we obtain $50 < A_V < 324$ mag.

Its notable that the ratio of IR polarization to visual extinction estimated using methods (2) and (3) covers a similar range for Cygnus A ($0.26 < P_K/A_V < 2.5$) and for 3C 433 ($0.47 < P_K^{int}/A_V < 2.9$). The fact that there is evidence for higher extinction in the case of Cygnus A helps to explain why its near-IR core source is relatively fainter than that detected in 3C 433.

Additional polarimetry observations at other near- and mid-IR wavelengths could help to distinguish among the three polarization mechanism mentioned above. In particular, comparison of our polarimetric measurements at 2.05 μm with those at both longer and shorter wavelengths could be used to distinguish between the scattering and dichroic polarization mechanisms. In the case of electron or optically thick dust scattering, we expect the polarization to show little variations across the near- and mid-IR bands, whereas the dichroic mechanism will produce a significant decline between *J* and *L* bands, following the Serkowski law (Serkowski 1973).

5 CONCLUSIONS

We have used *HST* and UKIRT observations to study 3C 433 at near-IR wavelengths, and have found several interesting features. The near-IR observations suggest that we are viewing the AGN directly through an obscuring dust structure perpendicular to the radio jets, or indirectly via scattering by a region close to the nucleus. On the other hand, the near-IR spectrum of the source shows a lack of broad lines. However, the estimated level of extinction ($3 < A_V < 67$ mag) and high intrinsic polarization of the nucleus (8.6 ± 1 per cent) support the idea that the high polarization may be due to dichroic extinction by a magnetized torus structure in the nuclear region of the galaxy.

It is now important to extend such studies to larger samples, in order to determine whether the polarization and extinction properties of 3C 433 are typical of the general population of powerful radio galaxies.

REFERENCES

Balmaverde B., Capetti A., Grandi P., 2006, A&A, 451, 35
Barker E. et al., 2007, NICMOS Instrument Handbook, Version 10.0. STScI, Baltimore
Barthel P. D., 1989, ApJ, 336, 606
Batcheldor D., Robinson A., Axon D., Hines D. C., Sparks W., Tadhunter C., 2006, PASP, 118, 642
Black A. R. S., Baum S. A., Leahy J. P., Perley R. A., Riley J. M., Scheuer P. A. G., 1992, MNRAS, 256, 186
Bohlin R. C., Savage B. D., Drake J. F., 1978, ApJ, 224, 132
Buttiglione S., Capetti A., Celotti A., Axon D. J., Chiaberge M., Macchetto F. D., Sparks W. B., 2009, A&A, 495, 1033
Capetti A., Axon D. J., Chiaberge M., Sparks W. B., Duccio Macchetto F., Cracraft M., Celotti A., 2007, A&A, 471, 137
Chiaberge M., Capetti A., Celotti A., 1999, A&A, 349, 77
Chiaberge M., Macchetto F. D., Sparks W. B., Capetti A., Allen M. G., Martel A. R., 2002, ApJ, 571, 247
Cohen M. H., Ogle P. M., Tran H. D., Goodrich R. W., Miller J. S., 1999, AJ, 118, 1963
de Koff S., Baum S. A., Sparks W. B., Biretta J., Golombek D., Macchetto F., McCarthy P., Miley G. K., 1996, ApJS, 107, 621
Demleitner M., Accomazzi A., Eichhorn G., Grant C. S., Kurtz M. J., Murray S. S., 2001, in Harnden F. R., Jr, Primini F. R., Dayne H. E., eds, ASP Conf. Ser. Vol. 238, Astronomical Data Analysis Software and Systems X. Astron. Soc. Pac., San Francisco, p. 321
Dicken D., Tadhunter C., Morganti R., Buchanan C., Oosterloo T., Axon D., 2008, ApJ, 678, 712
Djorgovski S., Weir N., Matthews K., Graham J. R., 1991, ApJ, 372, 67
Hardcastle M. J., Alexander P., Pooley G. G., Riley J. M., 1998, MNRAS, 296, 445
Hardcastle M. J., Evans D. A., Croston J. H., 2009, MNRAS, 396, 1929
Hill G. J., Goodrich R. W., DePoy D. L., 1996, ApJ, 462, 163
Holt J., Tadhunter C., Morganti R., Bellamy M., González Delgado R. M., Tzioumis A., Inskip K. J., 2006, MNRAS, 370, 1633
Holt J., Tadhunter C. N., González Delgado R. M., Inskip K. J., Rodriguez J., Emonts B. H. C., Morganti R., Wills K. A., 2007, MNRAS, 381, 611
Impey C., Gregorini L., 1993, AJ, 105, 853
Jones T. J., 1989, ApJ, 346, 728
Koski A. T., 1978, ApJ, 223, 56
Kriss G. A., 1988, ApJ, 324, 809
Krist J. E., Hook R., 2004, The Tiny Tim User's Guide, Version 6.3, STScI, Baltimore
Landt H., Bentz M. C., Ward M. J., Elvis M., Peterson B. M., Korista K. T., Karovska M., 2008, ApJS, 174, 282
Lilly S. J., Longair M. S., Miller L., 1985, MNRAS, 214, 109
MacLaughlin H., Wiklind T., 2007, NICMOS Data Handbook, http://www.stsci.edu/hst/nicmos
Madrid J. P. et al., 2006, ApJS, 164, 307s
Maiolino R., Marconi A., Salvati M., Risaliti G., Severgnini P., Oliva E., La Franca F., Vanzi L., 2001, A&A, 365, 28
Mathis J. S., 1990, ARA&A, 28, 37
Miller B. P., Brandt W. N., 2009, ApJ, 695, 755
Ogle P. M., Cohen M. H., Miller J. S., Tran H. D., Fosbury R. A. E., Goodrich R. W., 1997, ApJ, 482, 37
Ogle P. M., Whysong D., Antonucci R., 2006, ApJ, 647, 161
Osterbrock D. E., Koski A. T., Phillips M. M., 1976, ApJ, 206, 898
Rudy R. J., Tokunaga A. T., 1982, ApJ, 256, 1
Schlegel D. J., Finkbeiner D. P., Davis M., 1998, ApJ, 500, 525
Schmidt M., 1965, ApJ, 141, 1
Serkowski K., 1973, in Greenberg J. M., van de Hults H. C., eds, IAU Symp. 52, Interstellar Dust and Related Topics. Reidel, Dordrecht, p. 145
Simpson C., Rawlings S., 2000, MNRAS, 317, 1023
Simpson C., Ward M. J., Wilson A. S., 1995, ApJ, 454, 683
Sparks W. B., Axon D. J., 1999, PASP, 111, 1298
Tadhunter C. N., Packham C., Axon D. J., Jackson N. J., Hough J. H., Robinson A., Young S., Sparks W., 1999, ApJ, 512, 91
Tadhunter C. N. et al., 2000, MNRAS, 313, 52
Ueno S., Koyama K., Nishida M., Yamauchi S., Ward M. J., 1994, ApJ, 431, 1
van Breugel W., Balick B., Heckman T., Miley G., Helfand D., 1983, AJ, 88, 40
Whittet D. C. B., 1987, QJRAS, 28, 303
Wills K. A., Tadhunter C. N., Robinson T. G., Morganty R., 2002, MNRAS, 333, 211

This paper has been typeset from a T$_E$X/L^{A}T$_E$X file prepared by the author.